Radar Remote Sensing of Wetlands in Boreal Eurasia and North America for use in Methane Emission Modeling

Erika Podest[(1)], Kyle McDonald[(1)], Ted Bohn[(2)], Dennis Lettenmaier [(2)], M. Moghaddam[(3)], J. Whitcomb[(3)]

(1) Jet Propulsion Laboratory, California Institute of Technology, Pasadena, California; erika.podest@jpl.nasa.gov, kyle.mcdonald@jpl.nasa.gov

(2) University of Washington, Civil and Environmental Eng. Department, Seattle, Washington; tbohn@hydro.washington.edu, dennisl@u.washington.edu

(3) Dept. of Electrical Engineering and Computer Science, The University of Michigan, Ann Arbor, Michigan; mmoghadd@eecs.umich.edu, jbwhit@umich.edu

In the northern high latitudes, wetlands and open water bodies are common landscape features. Their carbon and methane emissions can have a large influence on hydrologic processes, surface-atmosphere carbon exchange, and associated impacts on global climate. It is therefore of great importance to assess their spatial extent and temporal character to improve hydrologic and ecosystem process modeling. SAR is an effective tool for this purpose because it is sensitive to surface water and it can monitor large inaccessible areas regardless of atmospheric conditions or solar illumination. We employ multi-temporal L-band SAR data from the Japanese satellites JERS-1 and PALSAR to map wetlands and open water bodies in Alaska and at a selection of study sites within the NEESPI domain, in Eurasia. A supervised decision tree based approach was used to generate the land cover products. For Alaska, we assembled regional-scale 100 m monthly JERS-1 mosaics from 1998 to assess open water change. DEM's and derived slope were also employed to improve classification performance in topographically complex regions where radar shadowing was prevalent. For selected basins in Eurasia, PALSAR and Landsat data were used in conjunction with JERS-1 imagery to map wetlands and open water change, at 30 m resolution. Products were validated with land cover and open water maps derived from Landsat, AVHRR, MODIS and SRTM. We examined methods for integrating these products within a hydrologic and methane modeling construct to investigate how wetland methane emissions respond to climate change.

Europe 100m JERS-1 Mosaic

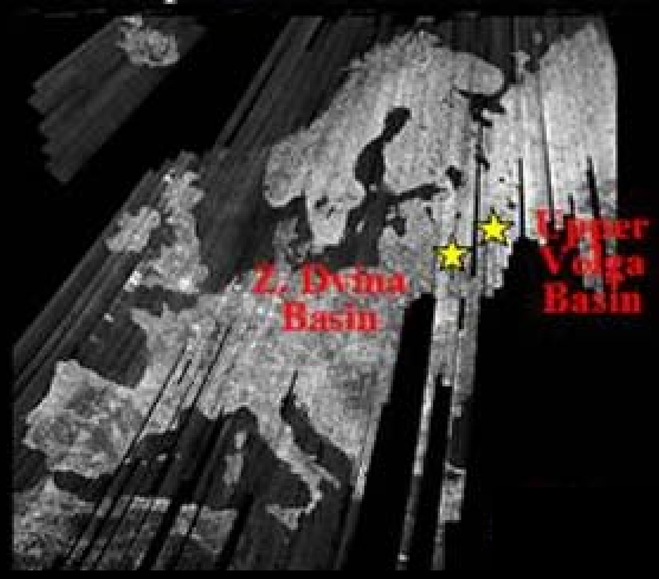

Eurasia 100m JERS-1 Mosaic

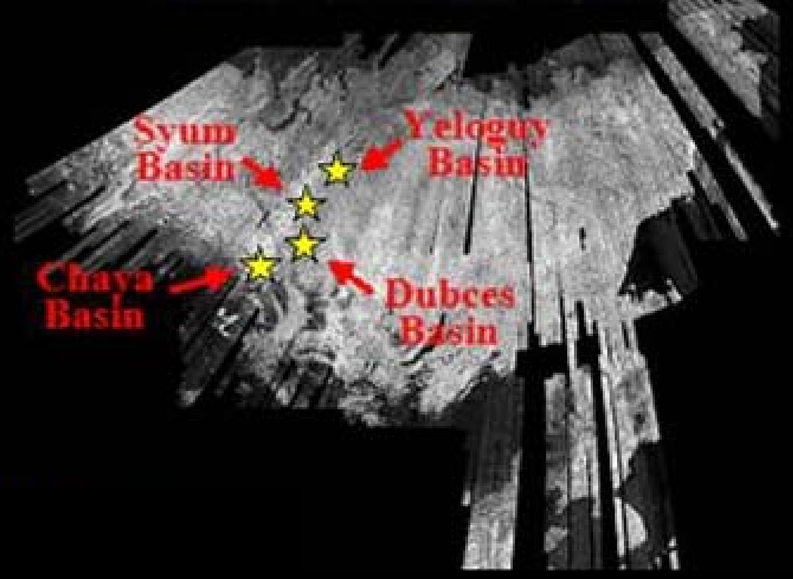

Alaska 100m JERS-1 Mosaic

This work was carried out at the Jet Propulsion Laboratory, California Institute of Technology, the University of Washington, and The University of Michigan under contract to the National Aeronautics and Space Administration.

Open Water Classification: Eurasia

Objective:
To produce a high resolution, 30 m, classification of open water bodies over focus basins in Eurasia using radar remote sensing.

Datasets:
Palsar (L-Band, 6.25 m, HH polarization); Landsat ETM (30 m); SRTM DEM (interpolated to 30 m). Ancillary products were derived from these datasets.

Approach:
A decision tree based approach was used to generate the open water maps based on the following input bands: Landsat band ratio of 5/2; ndvi; dem; derived slope; and radar backscatter.

Upper Volga Basin

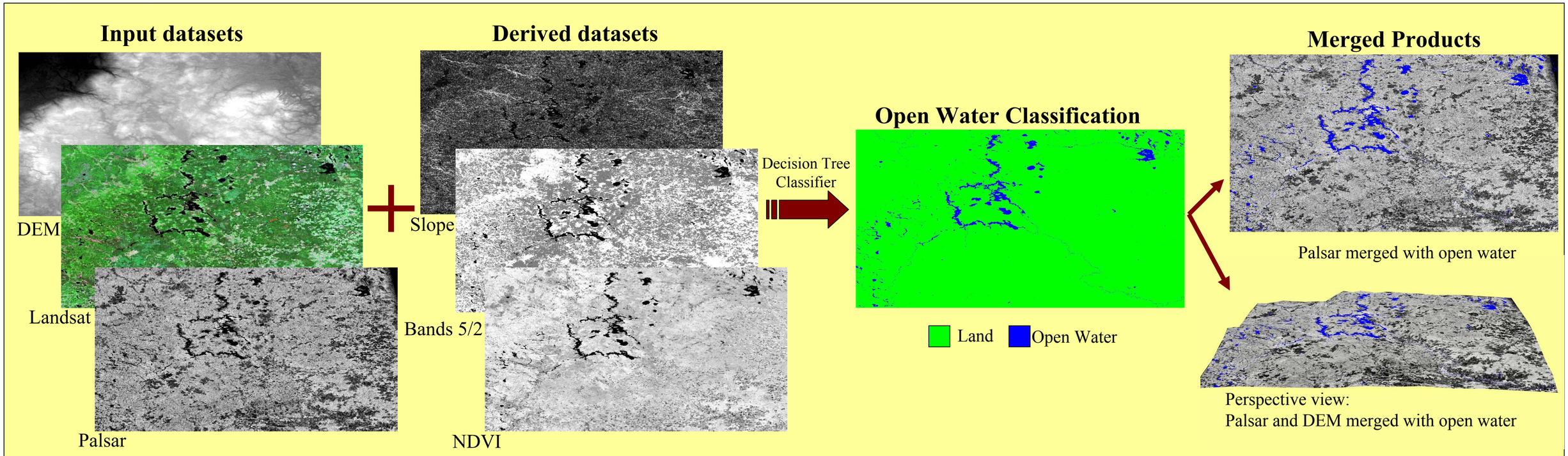

Synergy Between Optical and Radar

At L-band, open water appears very dark because it acts as a specular reflector. Areas with little or no vegetation also appear very dark and may be confused as open water. Optical wavelengths can differentiate bare surfaces from open water. However, cloud coverage is a common problem with optical data whereas radar data is impartial to it. The synergistic use of optical and radar data is of great advantage for detecting open water.

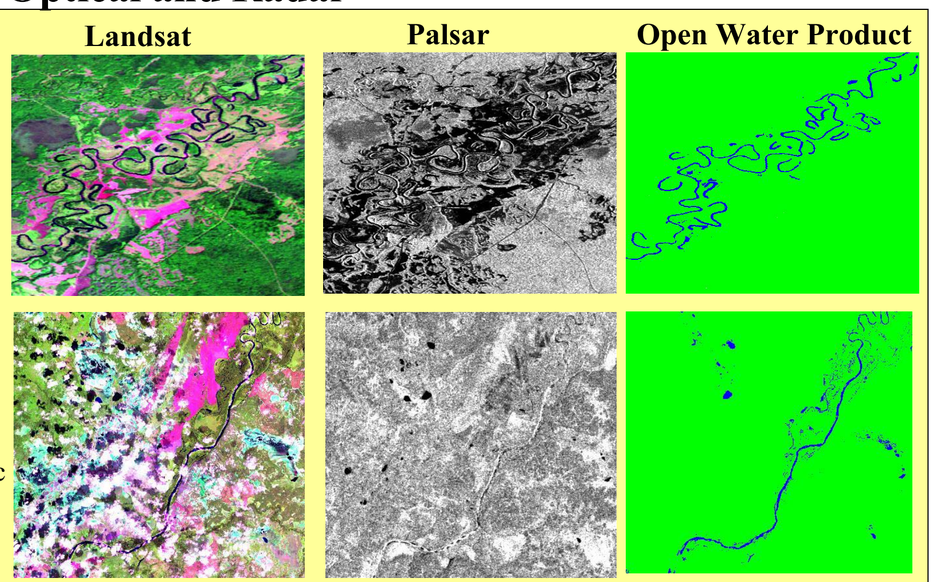

Open Water Classifications of the Different Basins

Illustration of Palsar and open water products for three different basins.

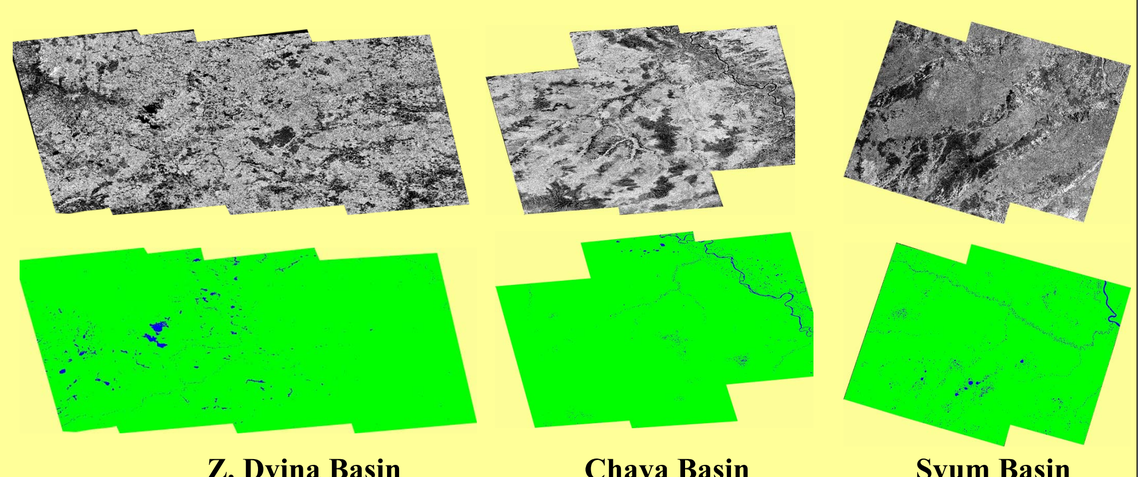

Wetland Classification: Eurasia

Objective:
To produce a high resolution, 30 m, wetlands classification over focus basins in Eurasia using radar remote sensing and ancillary datasets.

Datasets:
Palsar (L-Band, 6.25 m, HH); Landsat ETM (30 m); SRTM DEM (interpolated to 30 m). Ancillary products were derived from these datasets.

Approach:
A supervised decision tree based approach adapted from the Random Forest Algorithm (Breiman, 2001) was used.

Chaya Basin

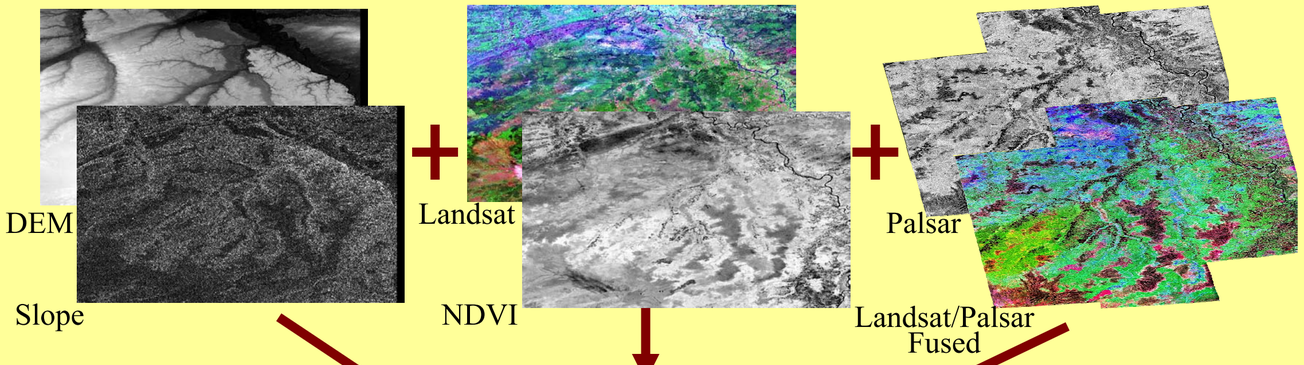

The above images and derived products have been coregistered to a common projection and 30 meter resolution. They serve as input layers into the decision tree classifier.

The open water classification generated previously was used to mask open water bodies

Image segmentation was applied using a classification software known as Ecognition.

Image Segmentation, Training data

Decision Tree Classifier

- High Biomass Forest - 52%
- Low Biomass Forest - 5%
- High Vegetation Wetland - 13%
- Low Vegetation Wetland - 18%
- Low Vegetation Saturated Wetland - 6%
- Open Water - 1%
- Agriculture/Nonforest - 5%

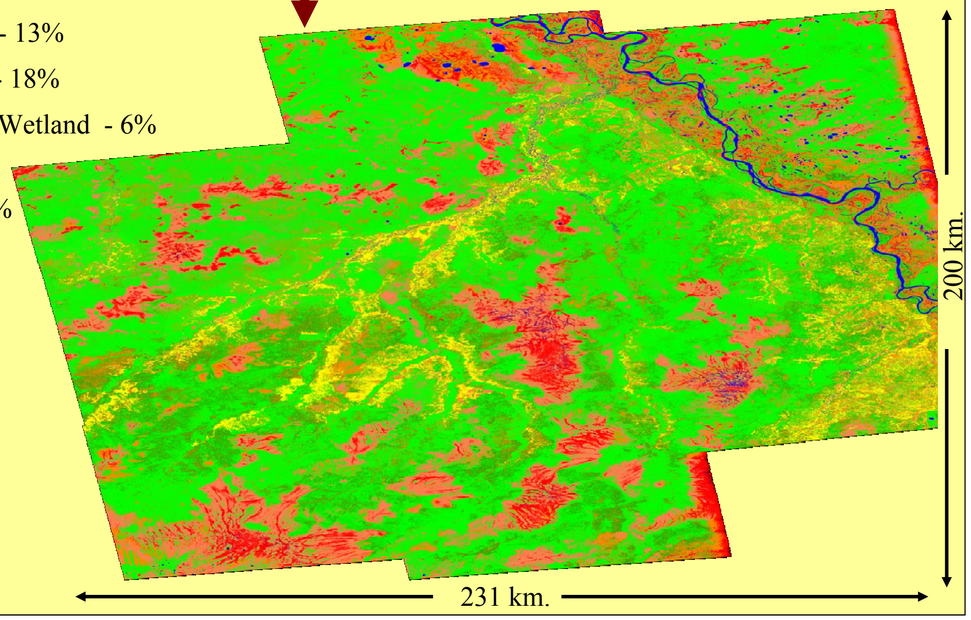

Accuracy assessment was based on validation pixels not used for training. Accuracy varied between 2% and 20% according to class. However, because of limited ground truth data, these values may vary.

Decision Tree Classifier: Random Forests

Random forest generates a large number of decision trees (i.e. a forest) based on ground reference (training) data and input data layers generated for remote sensing and ancillary data sources. Each decision tree is generated through an iterative process wherein nodes are split according to the pixel values in each input data layer covered by the training data. This continues until nodes can no longer be split. Each pixel to be classified is run through every decision tree in the forest. The final class assigned to the pixel is that class selected by the most decision trees in the forest. Classification accuracy is determined by comparing the final classified product to training data withheld during the generation of the forest.

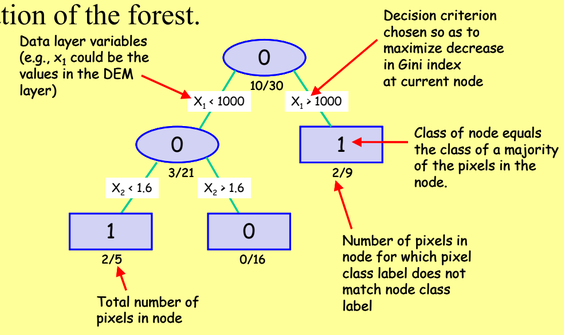

Assemble data layers

Mutually co-register data layers to common projection and 30 meter resolution

Derive ancillary products such as slope, ndvi, fusion of radar and optical

Create training file based on ground measurements

Apply image segmentation

Mask data layers to exclude open water

Set operating parameters and run Random Forest

Wetlands classification

Wetland Classifications of the Different Basins

Z. Dvina Basin

Syum Basin

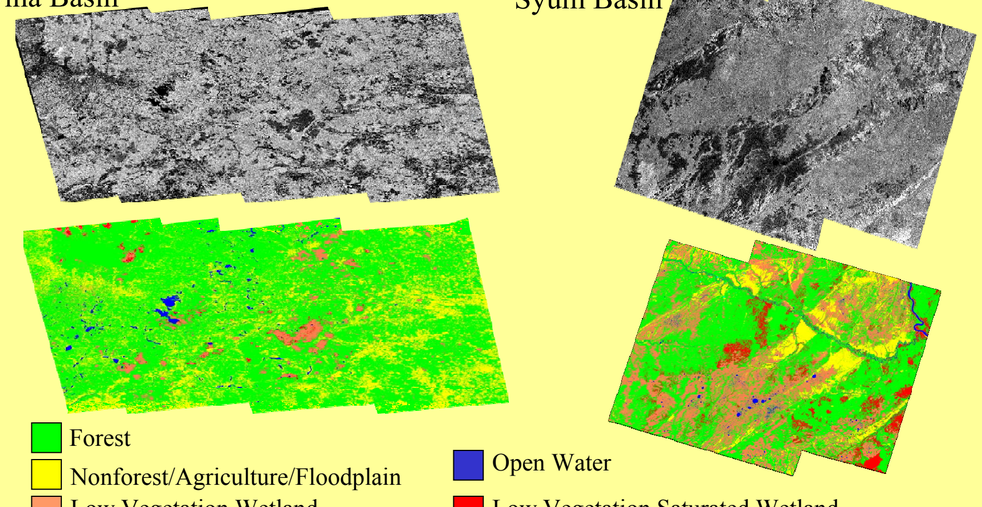

- Forest
- Nonforest/Agriculture/Floodplain
- Low Vegetation Wetland
- Open Water
- Low Vegetation Saturated Wetland

Open Water for Use in Methane Emissions Modeling

Objective:

To use 30 meter multi-temporal open water maps as input into a methane emissions model to assess how changes in open water affect methane emissions across a season.

Datasets and Models:

JERS-1 (L-Band, 12.5 m, HH); Landsat ETM (30 m); SRTM DEM (interpolated to 30 m).
Hydrogical model (VIC);
Ecosystem process model (BETHY); Walter and Heimann methane emissions model

Model Description

Our modeling framework consists of the Variable Infiltration Capacity (VIC) hydrological model (Liang *et al.*, 1994), enhanced with ecosystem processes taken from the Biosphere Energy Transfer Hydrology (BETHY) terrestrial carbon model (Knorr, 2000), and coupled to the wetland methane emissions model of Walter and Heimann (2000). The models are linked as follows: the VIC (enhanced with carbon cycling processes from the BETHY model (Knorr, 2000)) component runs at an hourly time step, simulating, among other variables, soil temperature, soil moisture, and net primary productivity (NPP). At the end of the simulation, these hourly time series are aggregated to daily values, and VIC's daily soil moisture is converted to a daily distribution of water table depths across the catchment. Then, for each day, the resulting distribution of water table depths is discretized, and methane emissions are estimated (via the methane emissions model of Walter and Heimann (2000)) as a function of soil temperature, NPP, and water table depth for each water table value in the discretized distribution. The total methane emission of the grid cell, then, is the area-weighted sum of the methane emissions from all of the discrete values of the water table depth.

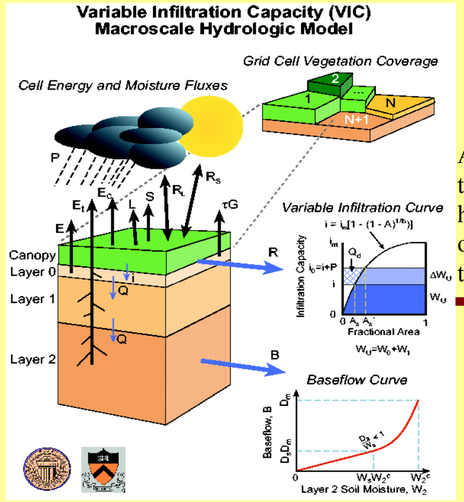

The VIC model:
1. Performs on large, "flat" grid cells (ex. 100x100 km.)
2. Generates hourly simulations of: soil temp., water table depth (Z_{WT}), NPP, other hydrologic variables

Spatial Hetergeneity: TOP-Model

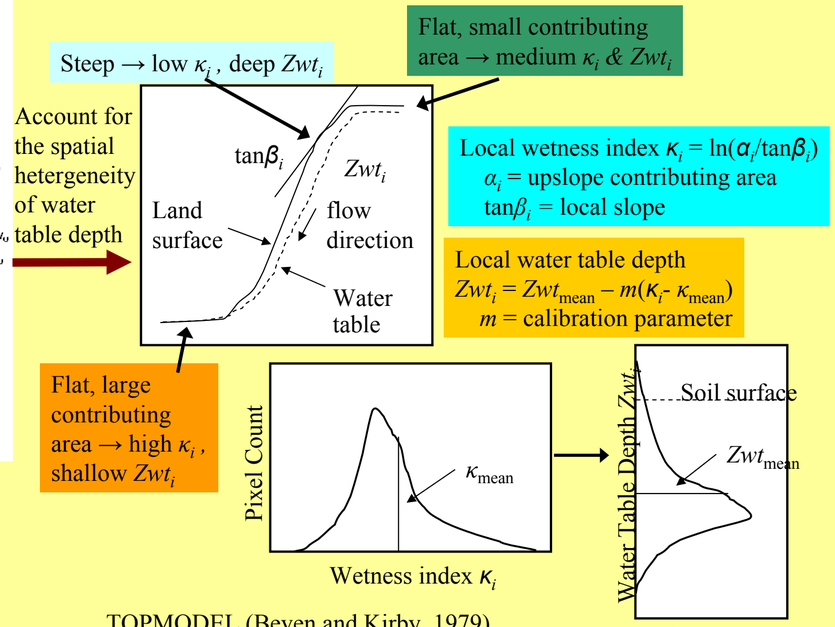

TOPMODEL (Beven and Kirby, 1979)

Process Flow

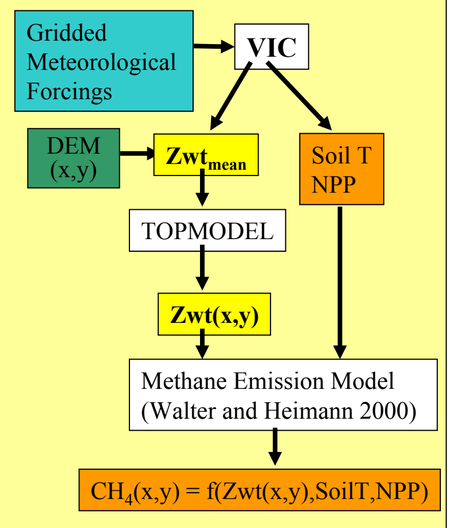

The above flowchart indicates the sequency of steps and input parameters needed to model methane emissions

Model Simulation: Chaya Basin

Multi-temporal JERS-1 data from 1995 were used to to produce open water maps. For the modeling component, two open water image swaths were chosen based on their overlap and day of acquisition. The first swath was acquired on April 10, 1995 (red) and the second on May 23, 1995 (yellow). These days represent wide variations in open water saturation.

Swath Coverage over the Chaya Basin

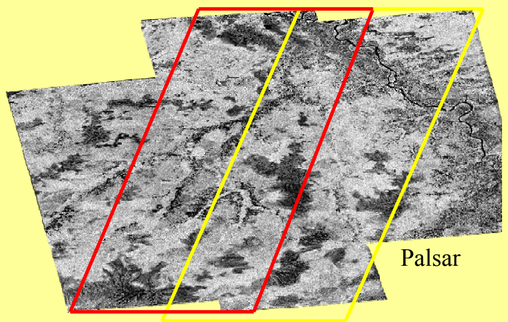

Red swath- April 10, 1995
Yellow swath- May 23, 1995

Multi-temporal Open Water Maps

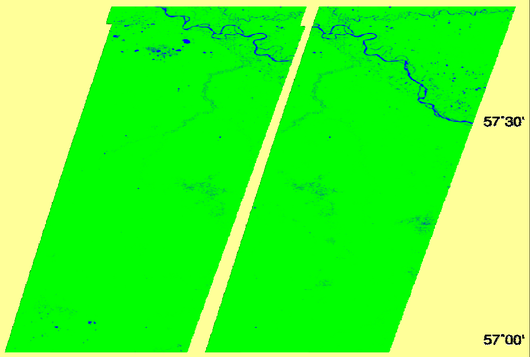

April 10, 1995 May 23, 1995

Change from day 100 to day 143 of 1995

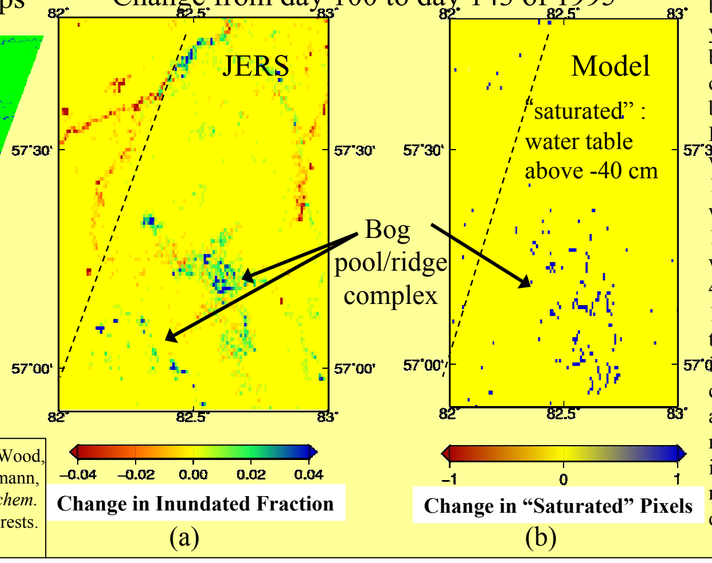

Change in saturated extent between day 100 and day 143, year 1995, given by JERS open water classification (a) and process-based modeling framework (b). Blue pixels in (a) contained open water on day 143 but not day 100. Red pixels contained open water on day 100 but not day 143. In panel (b), blue pixels had water table depth shallower than 40 cm below the surface on day 143 and deeper than 40 cm below the surface on day 100. Pixel size is 30 arc seconds. There is some correlation between simulated and observed saturation, but the model prediction could be improved by calibration with respect to the remote sensing observations.

References

Knorr, W., 2000, Annual and interannual CO_2 exchanges of the terrestrial biosphere: process-based simulations and uncertainties, *Global Ecol. Biogeogr.*, **9**, 225-252. ; Liang, X., Lettenmaier, D., Wood, E., and Burges. S,. 1994. A simple hydrologically based model of land surface water and energy fluxes for general circulation models, *J. Geophys. Res.,* **99**(D7), 14415-14428. ; Walter, B. and Heimann, M. 2000, A process-based, climate-sensitive model to derive methane emissions from natural wetlands: application to five wetland sites, sensitivity to model parameters, and climate, *Glob. Biogeochem. Cycles,* **14**(3), 745-765. ; Beven, K J, and Kirkby, M J, 1979, A physically based, variable contributing area model of basin hydrology, Hydrol. Sci. Bull., 24,43-69. ; Breiman, L., 2001. Random Forests. *Machine Learning,* **45**, 5-32. Open source software at: www.stat.berkley.edu/~brieman/randomforests.

Alaska Wetlands Map Derived from L-band JERS-1 SAR Mosaics

Ground Reference Data

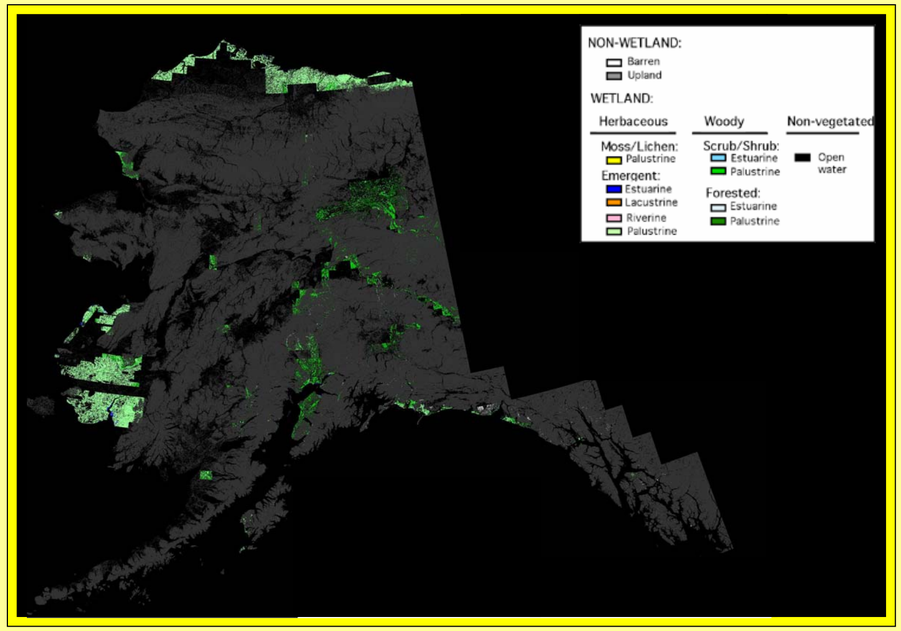

Ground reference data layer for Alaska (composite of NWI and AGDC databases). Although all classes shown in the legend are present in this ground reference set, some of them have a small number of pixels and are not visible at the resolution scale of this figure.

Example Input Data Layers

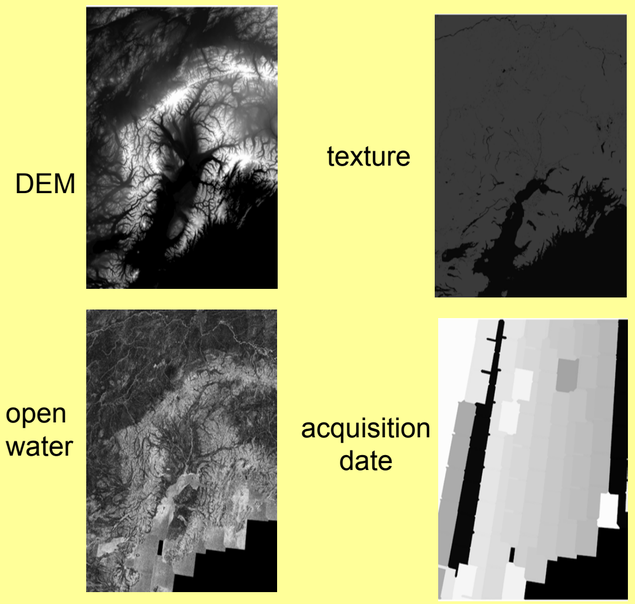

Data layers employed include maps of wetlands ground reference data, DEM, JERS-based open water maps, SAR acquisition date, image texture, proximity to water map.

Alaska Wetlands Map

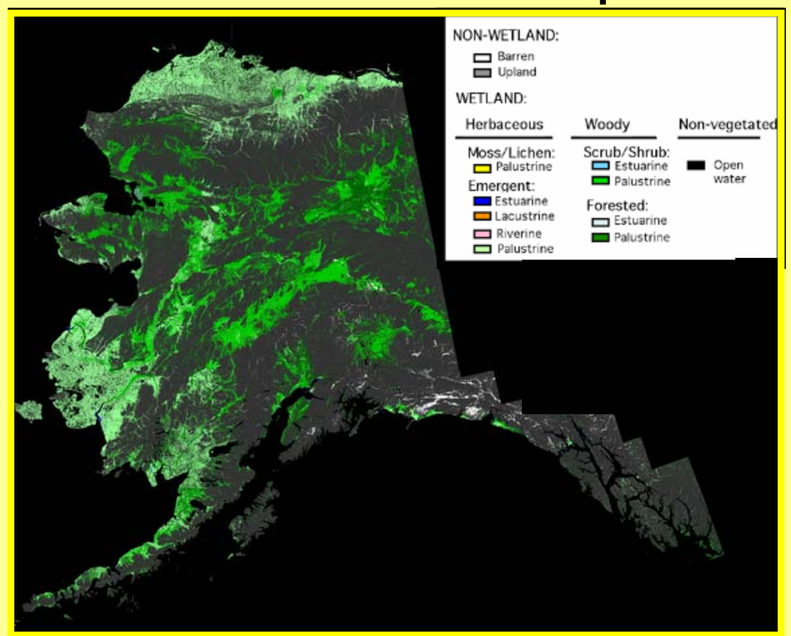

Whitcomb, Moghaddam, McDonald, Kellndorfer, and Podest, 2008 (in review).

Open Water Mapping

The Alaska JERS-1 mosaic was assembled with imagery from Summer 1998 when surface water is in a liquid state and in some cases at its maximum throughout the year. The USGS DEM was co-registered to the JERS-1 mosaic. It therefore has a resolution of 100m. Two classification approaches were applied, a supervised and an unsupervised approach. The DEM was used to mask out areas of high topography were shadowing was prevalent.

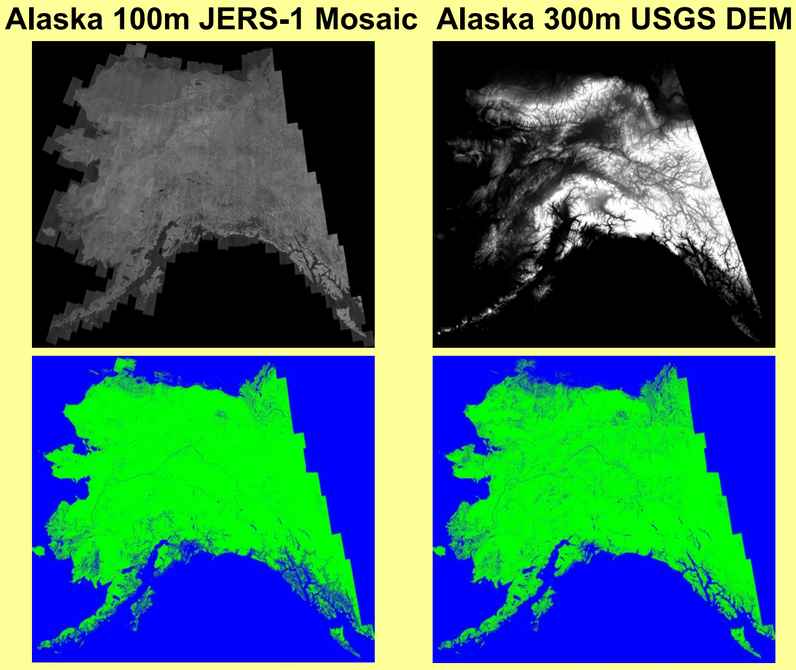

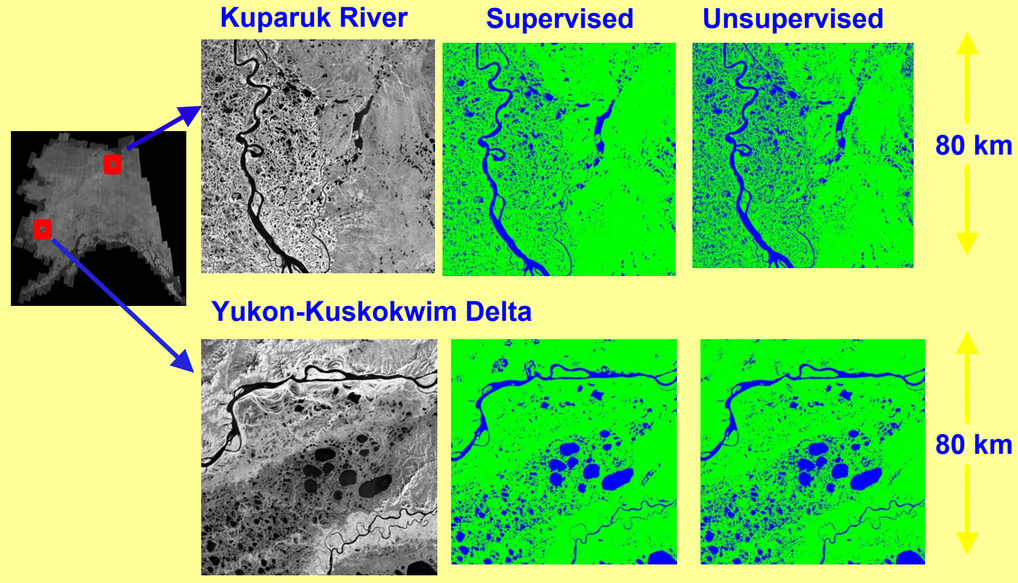

Within the 6400 km^2 region of the Kuparuk River, the supervised classification maps 14.5% of the landscape as open water, whereas the unsupervised technique shows 21.4% as open water. Within the Yukon-Kuskokwim Delta region, 16.5% and 15.0% are mapped as open water by the supervised and unsupervised techniques, respectively.

Alaska- Assessment of Monthly Open Water Change

An assessment of seasonal open water change was performed for Alaska. For this purpose, monthly JERS-1 mosaics were assembled at 100 meter resolution from January through October 1998, as shown on the right. A USGS DEM of the entire state was used to mask out areas of complex topography were radar shadowing was confused as open water. An supervised decision-tree based approach was applied. Open water change analysis was performed across areas with monthly overlaps where water was in a liquid state.

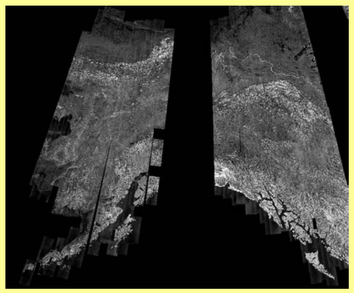
January 1998

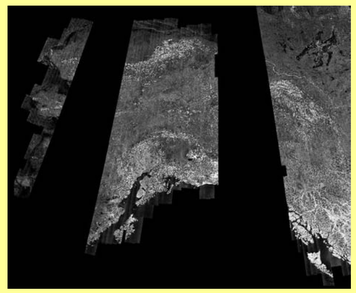
February 1998


March 1998


April 1998


May 1998


June 1998


July 1998


August 1998


September 1998


October 1998

Yukon Delta

An assessment in open water change was performed for the months of June, July, and September. The three images on the top right show open water (in blue) overlayed to the JERS image. The images on the bottom are comparisons of open water change relative to June. The table on the right shows the percent landcover change for July and September relative to June.

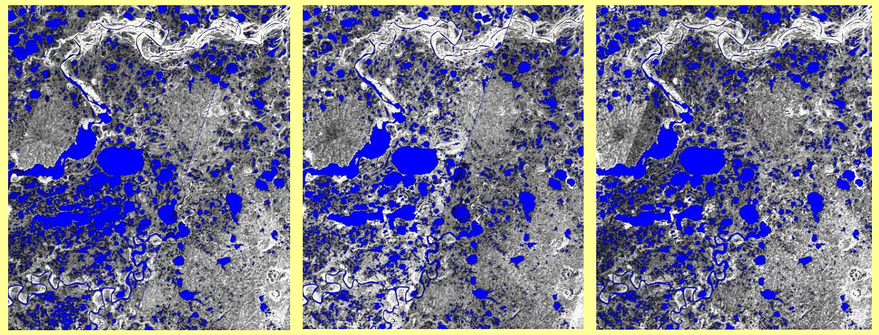

June 1998 July 1998 September 1998

More open water
Less open water
No change

Open Water Change Relative to June

	Dryer	Wetter
Jul.	5.2%	3.3%
Sep.	3.5%	3.3%

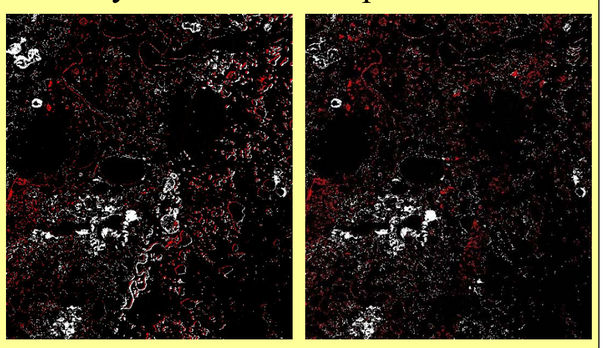
Open water change June/July

Open water change June/September

North Slope

Open water change was performed for the months of June, July, and August. The top shows open water overlayed on the JERS image and the bottom shows open water change relative to June.

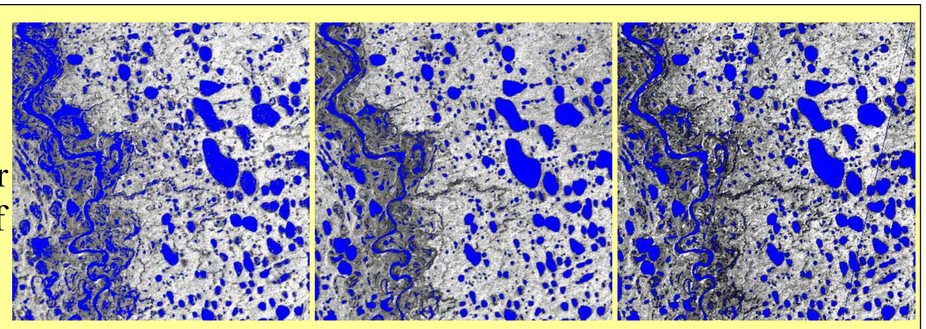
June 1998 July 1998 August 1998

Open Water Change Relative to June

	Dryer	Wetter
Jul.	7.7%	2.7%
Aug.	6.9%	3.2%

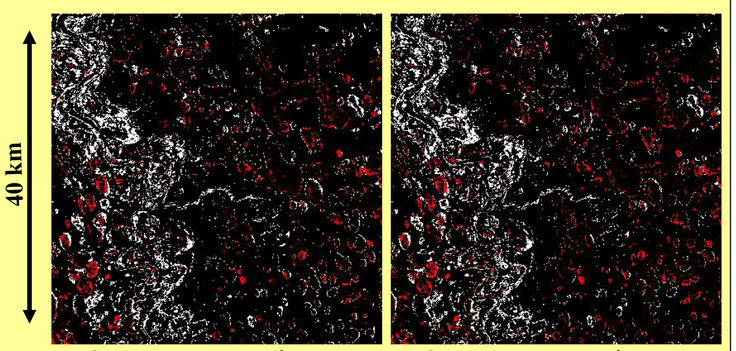

Open water change June/July

Open water change June/August